Article

Balanced Current Control Strategy for Current Source Rectifier Stage of Indirect Matrix Converter under Unbalanced Grid Voltage Conditions

Yeongsu Bak [1], June-Seok Lee [2] and Kyo-Beum Lee [1,*]

[1] Department of Electrical and Computer Engineering, Ajou University, 206, World cup-ro, Yeongtong-gu, Suwon 16499, Korea; wov2@ajou.ac.kr

[2] Railroad Safety Research Division, Korea Railroad Research Institute, 176, Cheoldo Bangmulgwan-ro, Uiwang-si, Gyeonggi-do 16105, Korea; ljs@krri.re.kr

* Correspondence: kyl@ajou.ac.kr; Tel.: +82-31-219-2487

Abstract: This paper proposes a balanced current control strategy for the current source rectifier (CSR) stage of an indirect matrix converter (IMC) under unbalanced grid voltage conditions. If the three-phase grid connected to the voltage source inverter (VSI) of the IMC has unbalanced voltage conditions, it affects the currents of the CSR stage and VSI stage, and the currents are distorted. Above all, the distorted currents of the CSR stage cause instability in the overall system, which can affect the life span of the system. Therefore, in this paper, a control strategy for balanced currents in the CSR stage is proposed. To achieve balanced currents in the CSR stage, the VSI stage should receive DC power without ripple components from the CSR stage. This is implemented by controlling the currents in the VSI stage. Therefore, the proposed control strategy decouples the positive and negative phase-sequence components existing in the unbalanced voltages and currents of the VSI stage. Using the proposed control strategy under unbalanced grid voltage conditions, the stability and life span of the overall system can be improved. The effectiveness of the proposed control strategy is verified by simulation and experimental results.

Keywords: indirect matrix converter (IMC); unbalanced voltage; positive phase-sequence component; negative phase-sequence component

1. Introduction

AC-AC power conversion systems are widely used in various applications such as renewable energy conversion systems, adjustable speed drives, and AC-AC transmission [1–5]. In general, a back-to-back (B2B) converter is used for AC-AC power conversion systems. It consists of a rectifier stage, inverter stage, and DC-link stage as energy storage elements. Therefore, a B2B converter is an AC-DC-AC indirect power conversion system; furthermore, it has disadvantages such as a bulky size and short lifetime because of the DC-link capacitors [6–10].

There is another topology for AC-AC power conversion: an indirect matrix converter (IMC). An IMC is structurally similar to a B2B converter; however, unlike the B2B converter, an IMC does not have energy storage elements such as DC-link capacitors. Therefore, an IMC can overcome the disadvantages of a B2B converter caused by the DC-link capacitors. An IMC is composed of a current source rectifier (CSR) stage as the input stage, and a voltage source inverter (VSI) stage as the output stage. It has a fictitious DC-link between the CSR stage and VSI stage. In this regard, the IMC is an AC-AC direct power conversion system, which is called a two-stage matrix converter. It has many advantages such as a compact power circuit and sinusoidal input and output currents under normal

conditions [11–15]. In general, the CSR stage of the IMC is connected to a three-phase voltage source such as three-phase grid and generation system (GS) using a generator or gas engine.

GSs are widely used in distributed GSs and microgrid systems [16–20]. The generator of a GS generates constant three-phase voltages in the normal state. In addition, power generated by the generator is transmitted to the three-phase grid of the output stage through a power conversion system such as a B2B converter or an IMC. In the IMC, if the three-phase grid of the output stage has balanced voltage conditions, the grid archives balanced three-phase currents. However, if the three-phase grid has unbalanced voltage conditions, the input and output currents are affected by the unbalanced grid voltage conditions and are distorted. The distorted currents of the input and output stages increase the torque ripple of the generator in the GS and degrade the power quality of the grid. This results in the instability of the overall system, and affects the life span of the system.

If the three-phase grid connected to the CSR stage of the IMC has unbalanced voltage conditions, the three-phase currents of the CSR stage are distorted. In order to reduce the distortion, the modulation strategies of the IMC under unbalanced voltage conditions of the three-phase grid connected to the CSR stage are researched [21,22].

This paper proposes a control strategy for balanced input currents of an AC-AC power conversion system using an IMC under unbalanced grid voltage conditions. Because the IMC does not have DC-link energy storage elements, the currents of the CSR stage are directly transmitted to the three-phase grid connected to the VSI stage. Therefore, under unbalanced grid voltage conditions, the currents of both the CSR stage and VSI stage are distorted. To control the balanced currents of the CSR stage, the power of the VSI stage transmitted from the CSR stage should be a DC value without ripple components because the voltages generated by the generator of the GS have balanced voltage conditions. The unbalanced voltages and currents of the VSI stage are composed of positive and negative phase-sequence components [23–25]. In the proposed control strategy, these are decoupled under unbalanced grid voltage conditions. These decoupled components are used to calculate new reference currents for balanced input currents, and the power quality of the grid can be improved using the proposed control strategy. Additionally, the distortion of the VSI stage currents caused by the unbalanced voltage conditions also decreases because of the proposed control strategy. The suitable operation and effectiveness of the proposed control strategy is demonstrated by simulation and experimental results.

2. Grid-Connected System Using Indirect Matrix Converter with Generation System

2.1. Overall System

Figure 1 shows a circuit diagram of the overall system, which is a grid-connected system using the IMC with the GS. The system is composed of four parts: the GS as a three-phase voltage source in the input stage, filter inductors and capacitors, IMC as a power conversion system, and a three-phase grid in the output stage. The generator of the GS generates constant three-phase voltages in normal state. The filter inductors and capacitors decrease the current and voltage ripple of the overall system.
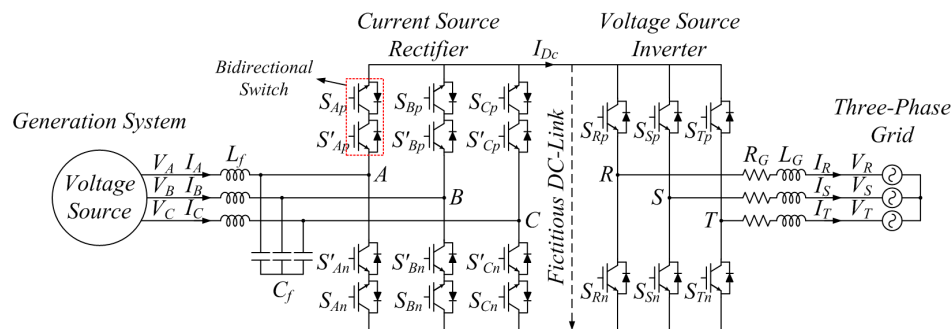

Figure 1. Circuit diagram of the overall system with generation system (GS), indirect matrix converter (IMC), and three-phase grid.

The IMC is an AC-AC power conversion system located between the GS of the input stage and three-phase grid of the output stage. Using the IMC, the power generated from the GS is transmitted to the three-phase grid. Additionally, the IMC is classified to the CSR stage connected to the GS and the VSI stage connected to the three-phase grid. The CSR and VSI stages are composed of 12 and 6 bidirectional switches, respectively. The IMC has a fictitious DC-link between the CSR and VSI stages.

2.2. Modulation Strategy of Current Source Rectifier Stage

In this paper, the modulation strategy of the CSR stage is equivalent to the conventional modulation strategy for the CSR stage of the IMC. The modulation of the CSR stage is performed to transmit the maximum voltage to the fictitious DC link from the generator as a three-phase voltage source. The fictitious DC-link voltage of the IMC is produced by the maximum and second largest magnitudes of the line-to-line voltages generated by the generator. The modulation strategy of the CSR stage is also required to maintain the sinusoidal currents and the unity power factor of the CSR stage [26].

Figure 2 shows a space vector diagram of the CSR. The space vectors of the CSR are classified into three null states and six active states. The three null states occur when the upper switches (S_{Xp} and $S'_{Xp} | X = A, B, C$) and lower switches (S_{Xn} and $S'_{Xn} | X = A, B, C$) in same phase leg are in the ON state simultaneously. In this case, the fictitious DC-link voltage is shorted to zero. Unlike the three null states, in the six active states, the power generated from the GS is transferred to the three-phase grid of the output stage.
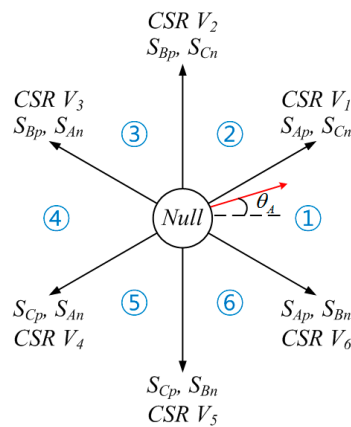

Figure 2. Space vector diagram of current source rectifier (CSR).

In Figure 2, a reference current phasor lying in sector 1 is reproduced by the reference currents (I_A^*, I_B^*, I_C^*) using the nearest vectors, which are *CSR V_1* and *CSR V_6*, as in Equation (1).

$$
\begin{aligned}
I_A^* &= I_m \cos \theta_A \quad (\theta_A = \omega_o t), \\
I_B^* &= I_m \cos \theta_B \quad \left(\theta_B = \theta_A - \tfrac{2\pi}{3}\right), \\
I_C^* &= I_m \cos \theta_C \quad \left(\theta_C = \theta_A - \tfrac{4\pi}{3}\right),
\end{aligned}
\tag{1}
$$

where I_m is the current amplitude, and θ_A, θ_B, and θ_C are the respective phase angles. Additionally, the active duty cycles (d_x and d_y) for the modulation of the CSR stage are expressed as in Equation (2).

$$
\cos \theta_A + \cos \theta_B + \cos \theta_C = 0, \quad -\frac{\cos \theta_B}{\cos \theta_A} - \frac{\cos \theta_C}{\cos \theta_A} = 1,
$$

$$
d_x = -\frac{\cos \theta_B}{\cos \theta_A}, \quad d_y = -\frac{\cos \theta_C}{\cos \theta_A}.
\tag{2}
$$

If the reference current phasor is located in sector 1, the average DC-link voltage ($V_{\text{DC}(av)}$) of the fictitious DC link produced by the maximum and second largest magnitudes of the line-to-line

voltages generated by the generator is expressed as in Equation (3). It is calculated by multiplying d_x, d_y, and the line-to-line voltages (V_{AB} and V_{CA}) of the CSR stage. It is represented as the phase voltage amplitude (V_m) and the power factor angle (ϕ_o) of the CSR stage.

$$V_{DC(av)} = d_x V_{AB} - d_y V_{CA} = \frac{3V_m}{2\cos\theta_A} \cdot \cos\phi_o \quad \left(-\frac{\pi}{6} \le \theta_A \le \frac{\pi}{6} \right). \tag{3}$$

2.3. Modulation Strategy of Voltage Source Inverter Stage

The VSI stage is similar to a three-phase two-level common inverter, which is composed of six switches. Figure 3 shows a space vector diagram of the VSI. The space vectors of the VSI are classified into two null states and six active states. The two null states are zero vectors such as *VSI* V_0 and *VSI* V_7.
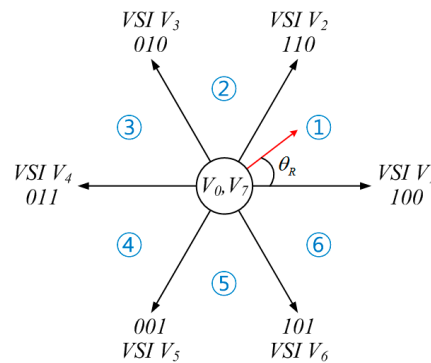

Figure 3. Space vector diagram of voltage source inverter (VSI).

In this paper, the VSI stage is modulated by a carrier-based pulse width modulation (PWM) method that compensates for the floating $V_{DC(av)}$ [27]. If the reference voltage phasor is located in sector 1, the two modulation signals [$v^*_{R(upper)}$ and $v^*_{R(lower)}$] in the *R* phase are expressed as in Equation (4).

$$v^*_{R(upper)} = -2d_y \cdot \frac{v_R + v_{offset}}{V_{DC(av)}} + d_x, \quad v^*_{R(lower)} = 2d_x \cdot \frac{v_R + v_{offset}}{V_{DC(av)}} - d_y, \tag{4}$$

where v_R is the *R*-phase reference voltage, and v_{offset} is the offset voltage of the three-phase reference voltages (v_R, v_S, v_T), which is expressed as in Equation (5).

$$v_{offset} = -\frac{1}{2} \cdot \left\{ max(v_R, \ v_S, \ v_T) + min(v_R, \ v_S, \ v_T) \right\}. \tag{5}$$

3. Proposed Control Strategy for Balancing Currents of Current Source Rectifier Stage under Unbalanced Grid Voltage Conditions

3.1. Control of Indirect Matrix Converter Connected to Three-Phase Grid

Figure 4 shows a control block diagram of the grid-connected system using the IMC. This system is composed of a GS connected to the CSR stage, and a three-phase grid connected to the VSI stage.

In the CSR stage, V_A, V_B, and V_C generated by the generator of the GS are transformed to a *d-q* axis synchronous reference frame using a phase angle (θ_{GS}), which is obtained from the rotation angle of the generator. The *d-q*-axis-transformed voltages of the CSR stage are used to select the CSR space vector and to calculate the duty cycles. Lastly, the switches of the CSR stage are operated by a modulation strategy with Equations (1)–(3).
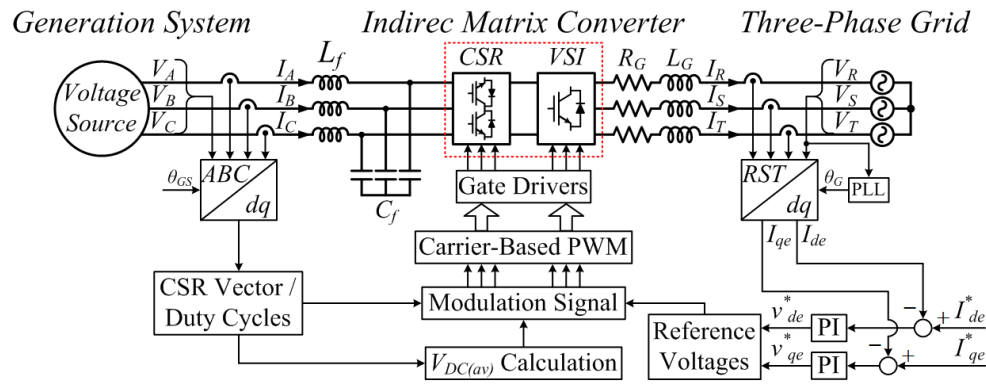
Figure 4. Control block diagram of grid-connected system using IMC.

In the VSI stage, a phase angle (θ_G) of the three-phase grid is generated by the phase-locked loop (PLL) method. The three-phase currents (I_R, I_S, I_T) are transformed to a *d-q* axis synchronous reference frame using θ_G. The *d-q* axis transformed currents (I_{de} and I_{qe}) of the VSI stage are controlled to *d-q* axis reference currents (I_{de}^* and I_{qe}^*) using proportional-integral (PI) control. Additionally, v_R, v_S, and v_T (as three-phase reference voltages) are produced by the current control. Lastly, the switches of the VSI stage are operated by the modulation strategy with Equations (4) and (5).

If the three-phase grid has balanced voltage conditions, in the normal state, the currents of the CSR stage and VSI stage are maintained as balanced three-phase currents. However, if the three-phase grid has unbalanced voltage conditions, the three-phase currents (I_A, I_B, I_C) of the CSR stage and I_R, I_S, and I_T of the VSI stage are distorted because the currents of the CSR stage are directly transmitted to the three-phase grid without the DC-link energy storage elements. In this case, an additional control strategy for balancing currents in the CSR stage is required under unbalanced grid voltage conditions because the distorted currents can affect the generator of the GS and decrease the power quality.

In this paper, the currents of the VSI stage are controlled to transmit DC power from the CSR stage to control the balanced currents of the CSR stage. In the proposed control strategy, the positive and negative phase-sequence components from the unbalanced grid voltages and currents are decoupled. In addition, these decoupled components are used to calculate the new reference currents for the positive and negative phase-sequence currents of the VSI stage. The decoupled positive and negative phase-sequence currents of the VSI stage are controlled as the new reference currents. This results in balanced currents in the CSR stage despite the unbalanced grid voltage conditions. Furthermore, the distortion of the VSI stage currents by the unbalanced voltage conditions decreases.

3.2. Decoupling the Positive and Negative Phase-Sequence Components from Unbalanced Grid Voltages and Currents

The unbalanced voltage conditions of the three-phase grid are generated by three-phase voltages with different magnitudes. The unbalanced grid voltages and currents involve the positive and negative phase-sequence components. In this regard, these components can be detected using a method of symmetrical coordinates [28]. Figure 5 shows the detection method for the positive and negative phase-sequence components from the unbalanced grid voltages and currents. First, 90° phase-shifted voltages and currents are generated by an orthogonal signal generator. The instantaneous values of the positive phase-sequence components (V_R^p, V_S^p, V_T^p, I_R^p, I_S^p, I_T^p) and the negative phase-sequence components (V_R^n, V_S^n, V_T^n, I_R^n, I_S^n, I_T^n) are detected using the voltages and currents (V_R, V_S, V_T, I_R, I_S, I_T) of the three-phase grid with 90° phase-shifted voltages and currents.
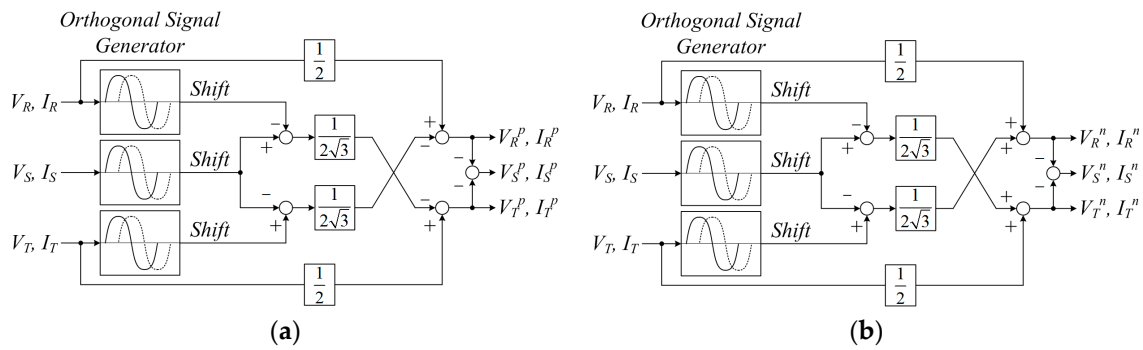
Figure 5. Detection method for positive and negative phase-sequence components from unbalanced grid voltages and currents. (**a**) Positive phase-sequence components; and (**b**) negative phase-sequence components.

3.3. Determination of Reference Currents for Balanced Currents of Current Source Rectifier Stage under Unbalanced Grid Voltage Conditions

In the grid-connected IMC with the GS, if the three-phase grid has unbalanced voltage conditions, the currents of the CSR stage and VSI stage are distorted. Therefore, new reference currents for the balanced currents of the CSR stage are required. In this paper, the detected positive and negative phase-sequence voltages and currents are used for the new reference currents of the VSI stage.

First, an angular frequency (ω) of V_R^p, V_S^p, and V_T^p is generated by the PLL method. V_R^p, V_S^p, and V_T^p, and I_R^p, I_S^p, and I_T^p under the unbalanced grid voltage conditions are transformed to a *d-q* axis synchronous reference frame (V_{dq}^p and I_{dq}^p) using ω. Additionally, *d-q* axis negative phase-sequence voltages (V_{dq}^n) and currents (I_{dq}^n) are transformed using a reverse angular frequency of the ω. In the grid-connected IMC, power generated by the generator of the GS is directly transmitted to the three-phase grid without the energy storage elements. Therefore, under unbalanced grid voltage conditions, the apparent electric power (*S*) generated by the generator of the GS can be calculated using V_{dq}^p, I_{dq}^p, V_{dq}^n, and I_{dq}^n as in Equation (6).

$$
\begin{aligned}
S &= \tfrac{3}{2} V_{dq} \overline{I_{dq}} = \tfrac{3}{2}\left(V_{dq}^p e^{j\omega t} + V_{dq}^n e^{-j\omega t} \right)\overline{\left(I_{dq}^p e^{j\omega t} + I_{dq}^n e^{-j\omega t} \right)}, \\
V_{dq}^p &= V_d^p + jV_q^p, \quad V_{dq}^n = V_d^n + jV_q^n, \\
I_{dq}^p &= I_d^p + jI_q^p, \quad I_{dq}^n = I_d^n + jI_q^n.
\end{aligned}
\tag{6}
$$

In addition, active [*P*(*t*)] and reactive instantaneous power [*Q*(*t*)] under unbalanced grid voltage conditions are calculated as in Equation (7). They are composed of DC components such as P_0 and Q_0 and AC components such as $P_{\cos 2}$, $P_{\sin 2}$, $Q_{\cos 2}$, and $Q_{\sin 2}$ vibrating to two times of the grid frequency.

$$
\begin{aligned}
P(t) &= P_0 + P_{\cos 2}\cos(2\omega t) + P_{\sin 2}\sin(2\omega t), \\
Q(t) &= Q_0 + Q_{\cos 2}\cos(2\omega t) + Q_{\sin 2}\sin(2\omega t).
\end{aligned}
\tag{7}
$$

P_0 and Q_0 as DC components and $P_{\cos 2}$, $P_{\sin 2}$, $Q_{\cos 2}$, and $Q_{\sin 2}$ as AC components are represented using V_{dq}^p, V_{dq}^n, I_{dq}^p, and I_{dq}^n as synchronous reference frame voltages and currents, as in Equation (8).

$$
\begin{aligned}
P_0 &= \tfrac{3}{2}\left(V_d^p I_d^p + V_q^p I_q^p + V_d^n I_d^n + V_q^n I_q^n \right), \\
P_{\cos 2} &= \tfrac{3}{2}\left(V_d^p I_d^n + V_q^p I_q^n + V_d^n I_d^p + V_q^n I_q^p \right), \\
P_{\sin 2} &= \tfrac{3}{2}\left(V_q^n I_d^p - V_d^n I_q^p - V_q^p I_d^n + V_d^p I_q^n \right), \\
Q_0 &= \tfrac{3}{2}\left(V_q^p I_d^p - V_d^p I_q^p + V_q^n I_d^n - V_d^n I_q^n \right), \\
Q_{\cos 2} &= \tfrac{3}{2}\left(V_q^p I_d^n - V_d^p I_q^n + V_q^n I_d^p - V_d^n I_q^p \right), \\
Q_{\sin 2} &= \tfrac{3}{2}\left(V_d^p I_d^n + V_q^p I_q^n - V_d^n I_d^p - V_q^n I_q^p \right).
\end{aligned}
\tag{8}
$$

From Equation (8), if $Q_{\cos 2}$ and $Q_{\sin 2}$ as AC components of the reactive power are eliminated to obtain balanced currents of the CSR stage through the balanced active power, the parameters of instantaneous power are rearranged in matrix form as in Equation (9). Therefore, the new reference currents are determined by V_{dq}^{p}; V_{dq}^{n}; active reference power such as P_0, $P_{\cos 2}$, and $P_{\sin 2}$; and Q_0 as the reactive reference power.

$$
\begin{bmatrix} \frac{2}{3}P_0 \\ \frac{2}{3}Q_0 \\ \frac{2}{3}P_{\cos 2} \\ \frac{2}{3}P_{\sin 2} \end{bmatrix} = \begin{bmatrix} V_d^p & V_q^p & V_d^n & V_q^n \\ V_q^p & -V_d^p & V_q^n & V_d^n \\ V_d^n & V_q^n & V_d^p & V_q^p \\ V_q^n & -V_d^n & -V_q^n & V_d^p \end{bmatrix} \begin{bmatrix} I_d^p \\ I_q^p \\ I_d^n \\ I_q^n \end{bmatrix}.
\tag{9}
$$

Additionally, to eliminate $P_{\cos 2}$ and $P_{\sin 2}$ as AC components of the active power under unbalanced grid voltage conditions, the reference power values are determined as in Equation (10).

$$
\begin{bmatrix} \frac{2}{3}P_0 & \frac{2}{3}Q_0 & \frac{2}{3}P_{\cos 2} & \frac{2}{3}P_{\sin 2} \end{bmatrix}^T = \begin{bmatrix} \frac{2}{3}P_{\text{out}} & \frac{2}{3}Q_{\text{out}} & 0 & 0 \end{bmatrix}^T.
\tag{10}
$$

If the reference power values are determined as in Equation (10), from Equation (9), the new reference currents for the balanced currents of the CSR stage under unbalanced grid voltage conditions are determined as in Equation (11). In addition, they are used for the *d-q* axis current controller of the VSI stage.

$$
\begin{bmatrix} I_d^p \\ I_q^p \\ I_d^n \\ I_q^n \end{bmatrix} = \begin{bmatrix} V_d^p & V_q^p & V_d^n & V_q^n \\ V_q^p & -V_d^p & V_q^n & V_d^n \\ V_d^n & V_q^n & V_d^p & V_q^p \\ V_q^n & -V_d^n & -V_q^n & V_d^p \end{bmatrix}^{-1} \begin{bmatrix} \frac{2}{3}P_{\text{out}} \\ \frac{2}{3}Q_{\text{out}} \\ 0 \\ 0 \end{bmatrix} = \frac{2P_{\text{out}}}{3A}\begin{bmatrix} V_d^p \\ V_q^p \\ -V_d^n \\ -V_q^n \end{bmatrix} + \frac{2Q_{\text{out}}}{3B}\begin{bmatrix} V_q^p \\ -V_d^p \\ V_q^n \\ -V_d^n \end{bmatrix},
$$

$$
I_d^{p*} = \frac{2V_d^p}{3A}P_{\text{out}}^* + \frac{2V_q^p}{3B}Q_{\text{out}}^*, \qquad I_q^{p*} = \frac{2V_q^p}{3A}P_{\text{out}}^* - \frac{2V_d^p}{3B}Q_{\text{out}}^*,
\tag{11}
$$

$$
I_d^{n*} = -\frac{2V_d^n}{3A}P_{\text{out}}^* + \frac{2V_q^n}{3B}Q_{\text{out}}^*, \quad I_q^{n*} = -\frac{2V_q^n}{3A}P_{\text{out}}^* - \frac{2V_d^n}{3B}Q_{\text{out}}^*,
$$

$$
A = \left[\left(V_d^p\right)^2 + \left(V_q^p\right)^2 \right] - \left[(V_d^n)^2 + (V_q^n)^2 \right], \quad B = \left[\left(V_d^p\right)^2 + \left(V_q^p\right)^2 \right] + \left[(V_d^n)^2 + (V_d^n)^2 \right].
$$

If the *d-q* axis reference currents under balanced grid voltage conditions are expressed as I_{de}^* and I_{qe}^*, they are indicated as active and reactive average powers, respectively. Therefore, the power references (P_{out}^* and Q_{out}^*) are expressed as in Equation (12).

$$
I_{qe}^* = \frac{2V_q^p}{3A}P_{\text{out}}^* \ \rightarrow \ P_{\text{out}}^* = \frac{3A}{2V_q^p}I_{qe}^*,
$$

$$
I_{de}^* = \frac{2V_q^p}{3B}Q_{\text{out}}^* \ \rightarrow \ Q_{\text{out}}^* = \frac{3B}{2V_q^p}I_{de}^*,
\tag{12}
$$

Substituting Equation (12) for Equation (11), the new reference currents for the balanced currents of the CSR stage under unbalanced grid voltage conditions are determined as in Equation (13), which are composed of the positive and negative phase-sequence voltages.

$$
I_d^{p*} = \frac{V_d^p}{V_q^p}I_{qe}^* + I_{de}^*, \qquad\qquad I_q^{p*} = I_{qe}^* - \frac{V_d^p}{V_q^p}I_{de}^*,
$$

$$
I_d^{n*} = -\frac{V_d^n}{V_q^p}I_{qe}^* + \frac{V_q^n}{V_q^p}I_{de}^*, \qquad I_q^{n*} = -\frac{V_q^n}{V_q^p}I_{qe}^* - \frac{V_d^n}{V_q^p}I_{de}^*.
\tag{13}
$$

Lastly, I_{dq}^p and I_{dq}^n (as decoupled positive and negative phase-sequence currents of the VSI stage) are controlled to new reference currents. In this regard, the new reference currents are calculated for the balanced active power by eliminating the AC components of P and Q under unbalanced grid voltage conditions. Therefore, the proposed control strategy leads to balanced currents of the CSR stage. In addition, the distortion of the VSI stage currents decreases.

4. Simulation Results

A comprehensive simulation study was performed using a Powersim (PSIM) simulation (Powersim Inc., Rockville, MD, USA) to verify the performance of the proposed control strategy for balancing currents of the CSR stage under unbalanced grid voltage conditions. In the simulation, the parameters of the elements in the overall system shown in Figure 1 are listed in Table 1.

Table 1. Parameters of elements in overall system.

Parameters	Value	Unit
L_f	0.0013	H
C_f	15	μF
R_G	0.1	Ω
L_G	0.004	H

Additionally, in the simulation, a permanent magnet synchronous generator (PMSG) is used to generate the three-phase voltages. Its parameters are listed in Table 2.

Table 2. Parameters of permanent magnet synchronous generator.

Parameters	Value	Unit
Stator resistance (R_s)	0.349	Ω
d-axis inductance (L_d)	0.01317	H
q-axis inductance (L_q)	0.0156	H
Permanent magnet flux (λ_s)	0.9218	Wb
Number of poles (P)	6	-
Moment of inertia (J)	0.02	kg·m^2

Figure 6 shows simulation results in which the three-phase currents of the VSI stage are controlled to reference current under balanced grid voltage conditions using the IMC. In this case, the PMSG of the GS is rotated at 750 rpm and generates three-phase 37.5-Hz/190-V$_\text{peak}$ line-to-line voltages such as V_AB, V_BC, and V_CA. V_DC of the IMC is generated by the maximum and second-largest magnitudes of V_AB, V_BC, and V_CA generated by the PMSG. To produce V_DC, the CSR stage of the IMC is controlled using a modulation strategy. The three-phase grid generates three-phase 60-Hz/50-V$_\text{rms}$ line-to-line voltages such as V_RS, V_ST, and V_TR. In addition, I_R, I_S, and I_T are controlled to 3 A through the IMC. The three-phase currents of the CSR and VSI stages are generated to balance currents because the three-phase grid has balanced voltage conditions.

Figure 7 shows simulation results in which the positive and negative phase-sequence voltages of the VSI stage under unbalanced grid voltage conditions are detected. The three-phase grid is changed to unbalanced voltage conditions at 0.1 s from the normal state, with balanced voltage conditions supplying three-phase 60-Hz/50-V$_\text{rms}$ line-to-line voltages. In this case, the magnitude of V_R decreases to 70% compared with that of the normal state. Depending on the detection method as shown in Figure 5, V_R^p, V_S^p, and V_T^p (as the positive phase-sequence voltages) and V_R^n, V_S^n, and V_T^n (as negative phase-sequence voltages) are detected under unbalanced grid voltage conditions. These detected values are used to calculate the new reference currents for the positive and negative phase-sequence currents of the VSI stage.
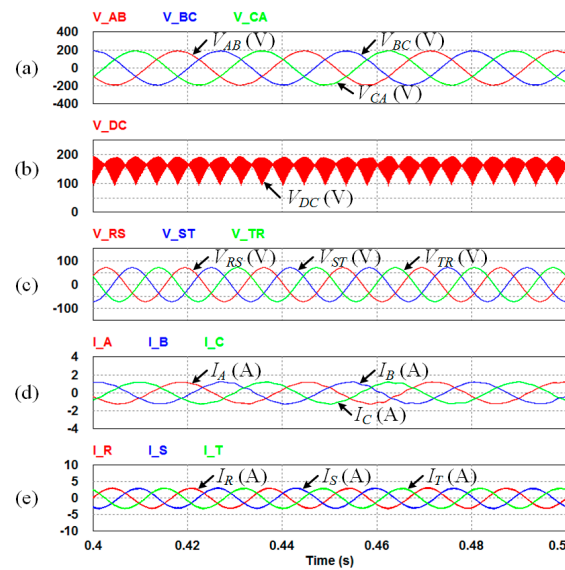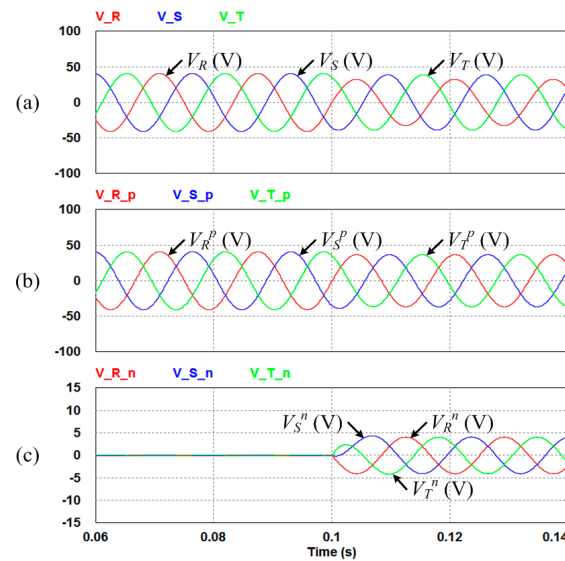
Figure 6. Simulation results where three-phase currents of VSI stage are controlled to reference current under balanced grid voltage conditions. (**a**) Line-to-line voltages (V_{AB}, V_{BC}, V_{CA}) of the permanent magnet synchronous generator (PMSG); (**b**) fictitious DC-link voltage (V_{DC}); (**c**) line-to-line voltages (V_{RS}, V_{ST}, V_{TR}) of the three-phase grid; (**d**) three-phase currents (I_A, I_B, I_C) of the CSR stage; and (**e**) three-phase currents (I_R, I_S, I_T) of the VSI stage.

Figure 7. Simulation results where positive and negative phase-sequence voltages of VSI stage under unbalanced grid voltage conditions are detected. (**a**) Phase voltages (V_R, V_S, V_T) of the three-phase grid; (**b**) positive phase-sequence voltages (V_R^p, V_S^p, V_T^p); and (**c**) negative phase-sequence voltages (V_R^n, V_S^n, V_T^n).

Figure 8 shows simulation results in which the three-phase currents of the CSR and VSI stages are distorted depending on the unbalanced grid voltage conditions. In the same scenario as that of Figure 6, the PMSG and three-phase grid generate three-phase 37.5-Hz/190-V_{peak} line-to-line voltages and three-phase 60-Hz/50-V_{rms} line-to-line voltages, respectively. In addition, I_R, I_S, and I_T are controlled to 3 A using the IMC. However, the three-phase grid is changed to unbalanced voltage conditions at 0.1 s. The V_R is decreased to 70% compared with that of the normal state. Therefore, I_A, I_B, and I_C (as the three-phase currents of the CSR stage) and I_R, I_S, and I_T (as the three-phase currents

of the VSI stage) are distorted. As the distorted currents can affect the GS, three-phase grid, and overall system, a control strategy for balancing currents of the CSR and VSI stages is required. In this paper, a control strategy using the positive and negative phase-sequence voltages and currents is proposed for balancing currents of the CSR stage.
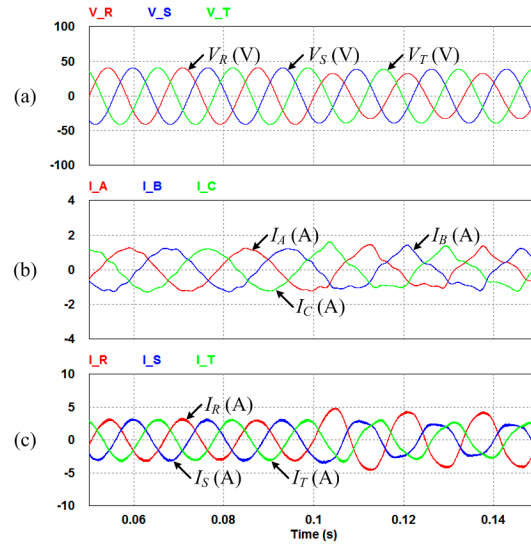

Figure 8. Simulation results where three-phase currents of CSR and VSI stages are distorted depending on unbalanced grid voltage conditions. (**a**) V_R, V_S, and V_T of the three-phase grid; (**b**) I_A, I_B, and I_C of the CSR stage; and (**c**) I_R, I_S, and I_T of the VSI stage.

Figure 9 shows simulation results in which the three-phase currents of the CSR stage are controlled to balance currents using the proposed control strategy under unbalanced grid voltage conditions. It has the same scenario as that of Figure 8. Depending on the proposed control strategy using the new reference currents for the balanced currents of the CSR stage, the distortion of the CSR stage currents decreases. Additionally, the distortion of the VSI stage currents also decreases because the IMC does not have DC-link energy storage elements.
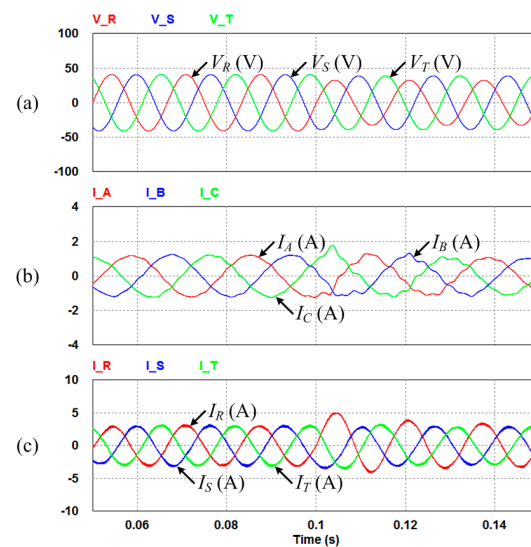

Figure 9. Simulation results in which three-phase currents of CSR stage are controlled to balance currents using proposed control strategy under unbalanced grid voltage conditions. (**a**) V_R, V_S, and V_T of the three-phase grid; (**b**) I_A, I_B, and I_C of the CSR stage; and (**c**) I_R, I_S, and I_T of the VSI stage.

5. Experiment Results

Experiments were performed using the experimental setup shown in Figure 10 to verify the performance of the proposed control strategy for balanced currents of the CSR stage under unbalanced grid voltage conditions. The experimental setup consists of a control board, power board, and sensors. The control board is composed of a digital signal processor (DSP) using the TMS320C28346 and a field-programmable gate array (FPGA). The power board is composed of a rectifier stage and an inverter stage using the IGBT switches and gate drivers. Additionally, the PMSG of the GS is connected to an induction motor (IM), which is operated by a common inverter to drive at constant speed. The parameters of the PMSG are equal to those of the simulation listed in Table 2.
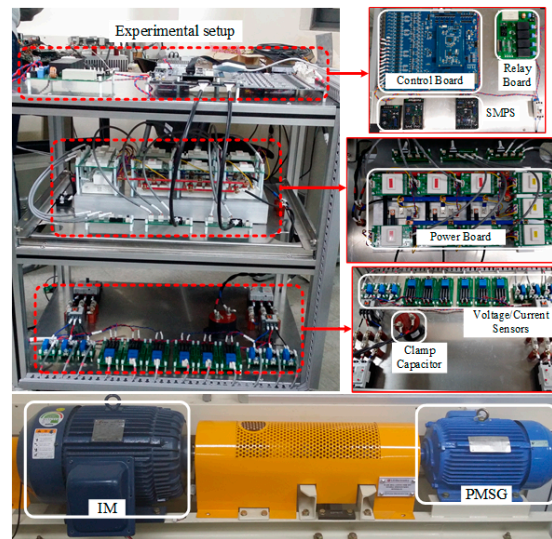
Figure 10. Experimental setup and PMSG with induction motor (IM).

Figure 11a,b shows experimental results where the three-phase currents of the VSI stage are controlled to reference current under balanced grid voltage conditions. It has same scenario as that of Figure 6. The PMSG of the GS generates three-phase 37.5-Hz/190-V_{peak} line-to-line voltages such as V_{AB}. The three-phase grid generates three-phase 60-Hz/50-V_{rms} line-to-line voltages such as V_{RS}, V_{ST}, and V_{TR}. Additionally, I_R, I_S, and I_T (as the three-phase currents of the VSI stage) are controlled to 3 A through the IMC. In this case, I_A, I_B, and I_C (as the three-phase currents of the CSR stage) and I_R, I_S, and I_T are generated to balance currents because the three-phase grid has balanced voltage conditions.
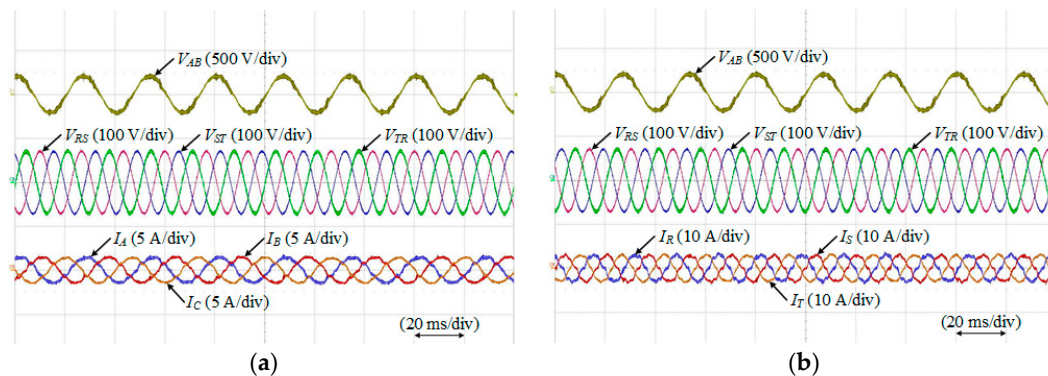

(a)　　　　　　　　　　　　　　　　　　　　(b)

Figure 11. Experimental results in which three-phase currents of VSI stage are controlled to reference current under balanced grid voltage conditions. (**a**) Balanced currents of CSR stage; and (**b**) balanced currents of VSI stage.

Additionally, experimental results for V_{AB}, V_{BC}, and V_{CA} generated by the PMSG and the V_{DC} as the fictitious DC-link voltage are shown in Figure 12. The V_{DC} of the IMC is generated by the maximum and second-largest magnitudes of V_{AB}, V_{BC}, and V_{CA}.
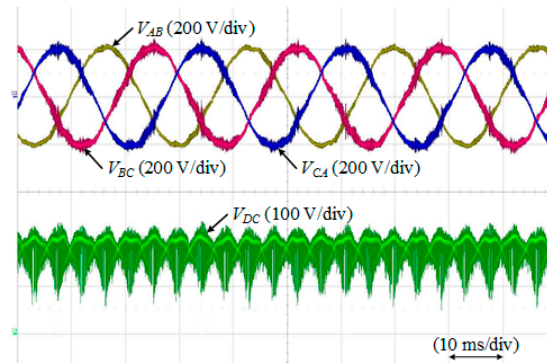

Figure 12. Experimental results of line-to-line voltages generated by PMSG and fictitious DC-link voltage.

Figure 13a,b shows experimental results where the positive and negative phase-sequence voltages of the VSI stage under unbalanced grid voltage conditions are detected. The three-phase grid is changed to unbalanced voltage conditions from the normal state; in other words, the magnitude of V_R as the R-phase voltage is decreased to 70% compared with that of the normal state. Depending on the detection method, V_R^p, V_S^p, and V_T^p (as the positive phase-sequence voltages) and V_R^n, V_S^n, and V_T^n (as negative phase-sequence voltages) are detected. They are required to calculate the new reference currents in the proposed control strategy for balanced currents of the CSR stage under unbalanced grid voltage conditions.
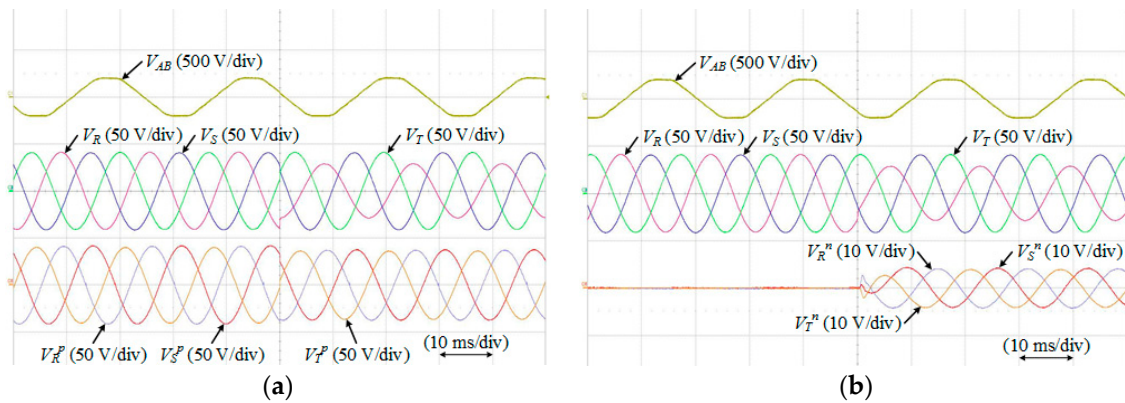

(a)

(b)

Figure 13. Experimental results with positive and negative phase-sequence voltages of VSI stage under unbalanced grid voltage conditions. (**a**) Detection of positive phase-sequence voltages; and (**b**) detection of negative phase-sequence voltages.

In the same scenario as that of Figure 8, if the three-phase grid has unbalanced voltage conditions, the three-phase currents of the CSR and the VSI stages are distorted. These are shown in Figure 14a,b, respectively. In this case, I_R, I_S, and I_T are controlled to 3 A using the IMC. However, the three-phase grid is changed to unbalanced voltage conditions where V_R is decreased to 70% compared with that of the normal state. Therefore, I_A, I_B, and I_C (as the three-phase currents of the CSR stage) and I_R, I_S, and I_T (as the three-phase currents of the VSI stage) are distorted. These currents can affect the overall system. Therefore, in this paper, the proposed control strategy with positive and negative phase-sequence voltages and currents is used to balance currents of the CSR stage.

Figure 15a,b shows experimental results where the three-phase currents of the CSR stage are controlled to balance currents using the proposed control strategy under unbalanced grid voltage conditions. Although the three-phase grid has unbalanced voltage conditions, I_A, I_B, and I_C (as the three-phase currents of the CSR stage) and I_R, I_S, and I_T (as the three-phase currents of the VSI stage) are controlled to balance currents depending on the proposed control strategy. The distortion of the CSR stage and the VSI stage currents decreases compared with that of Figure 14.
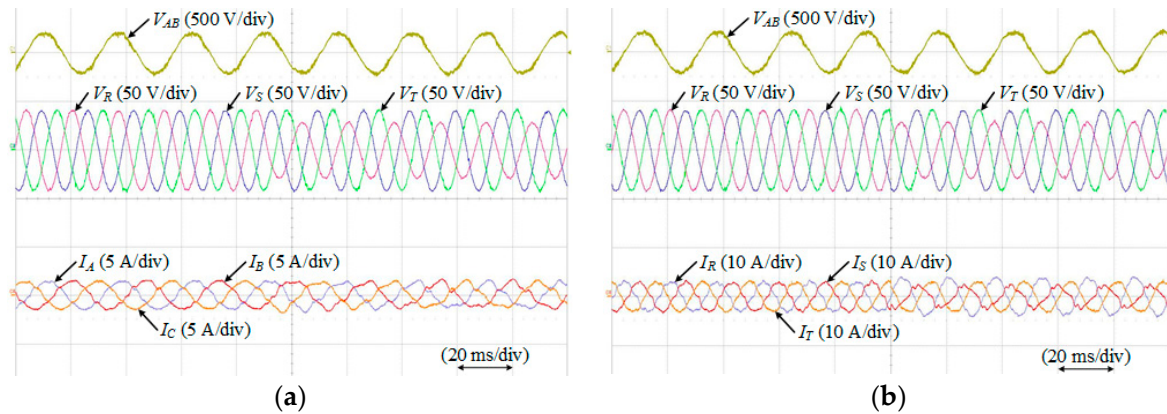
Figure 14. Experimental results in which three-phase currents of CSR and VSI stages are distorted by unbalanced voltage conditions. (**a**) Distorted currents of CSR stage; and (**b**) distorted currents of VSI stage.
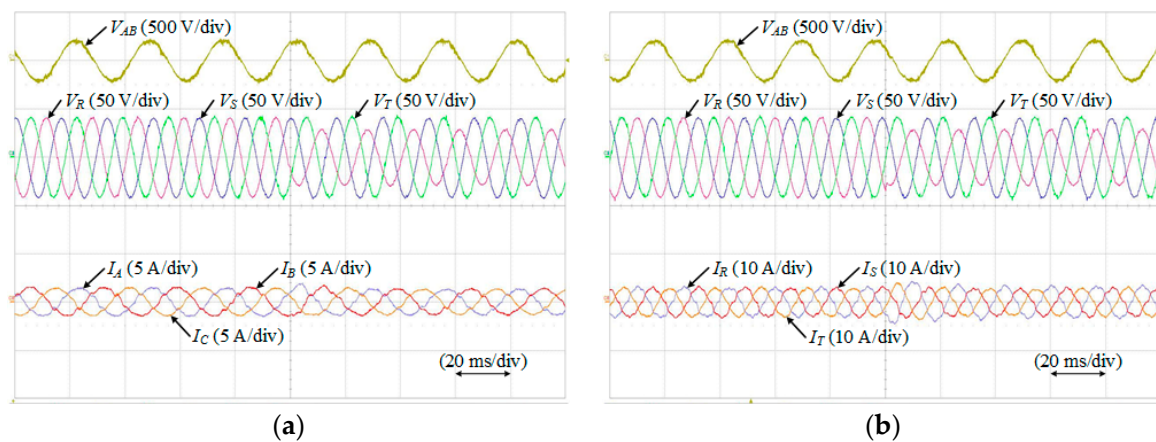

Figure 15. Experimental results in which three-phase currents of CSR stage are controlled to balance currents using proposed control strategy under unbalanced grid voltage conditions. (**a**) Balanced currents of CSR stage; and (**b**) balanced currents of VSI stage.

In addition, Figure 16a,b shows experimental results where the three-phase currents of the CSR and the VSI stages are distorted under unbalanced grid voltage conditions. In this case, I_R, I_S, and I_T are controlled to 3 A using the IMC. However, the three-phase grid is changed to unbalanced voltage conditions where V_R and V_S are decreased to 70% compared with those of the normal state. Therefore, the three-phase currents of the CSR and the VSI stages are distorted.
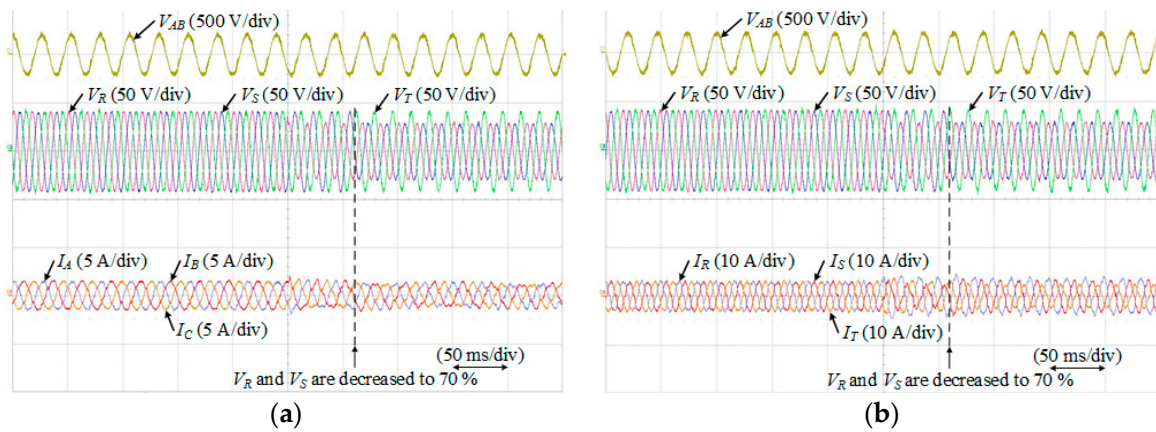
Figure 16. Experimental results in which three-phase currents of CSR and VSI stages are distorted by unbalanced voltage conditions depending on decrease in two-phase grid voltages. (**a**) Distorted currents of CSR stage; and (**b**) distorted currents of VSI stage.

In the same scenario as that of Figure 16a,b, Figure 17a,b shows experimental results where the three-phase currents of the CSR stage are controlled to balance currents using the proposed control strategy under unbalanced grid voltage conditions depending on decreases in two-phase grid voltages. Although the three-phase grid has unbalanced voltage conditions, I_A, I_B, and I_C (as the three-phase currents of the CSR stage) and I_R, I_S, and I_T (as the three-phase currents of the VSI stage) are controlled to balance currents using the proposed control strategy.
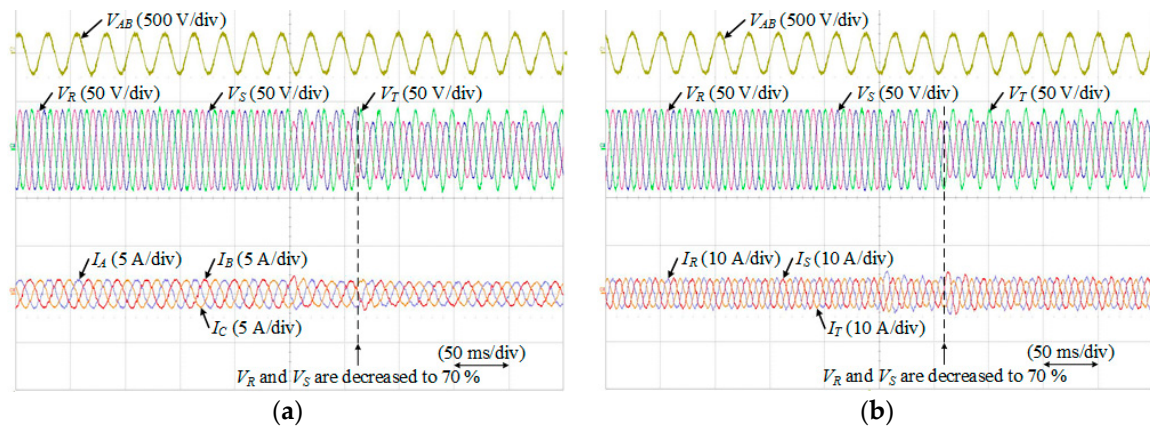

Figure 17. Experimental results in which three-phase currents of CSR stage are controlled to balance currents using proposed control strategy under unbalanced grid voltage conditions, depending on decrease in two-phase grid voltages. (**a**) Balanced currents of CSR stage; and (**b**) balanced currents of VSI stage.

Additionally, total harmonic distortion (THD) analysis for the three-phase currents of the CSR and VSI stage are progressed depending on the grid voltage condition and the control strategy. Figure 18a–c shows experimental results of THD analysis for the three-phase currents of the CSR stage such as I_A, I_B, and I_C and fast Fourier transform (FFT) spectrum of I_A. They have same scenario as that of Figure 11a, Figure 14a, and Figure 15a, respectively. In Figure 18a, the three-phase grid has balanced voltage conditions and the three-phase current of the VSI stage are controlled to reference current using the general control strategy. However, in Figure 18b,c, the three-phase grid has unbalanced voltage conditions depending on decreasing of the magnitude of V_R compared with that of the normal state. Therefore, I_A, I_B, and I_C are distorted and THDs of them are increased as shown in Figure 18b.

In Figure 18c, the three-phase currents of the VSI stage are controlled using the proposed control strategy for the balanced currents of the CSR stage. As a result, THDs of I_A, I_B, and I_C are decreased.
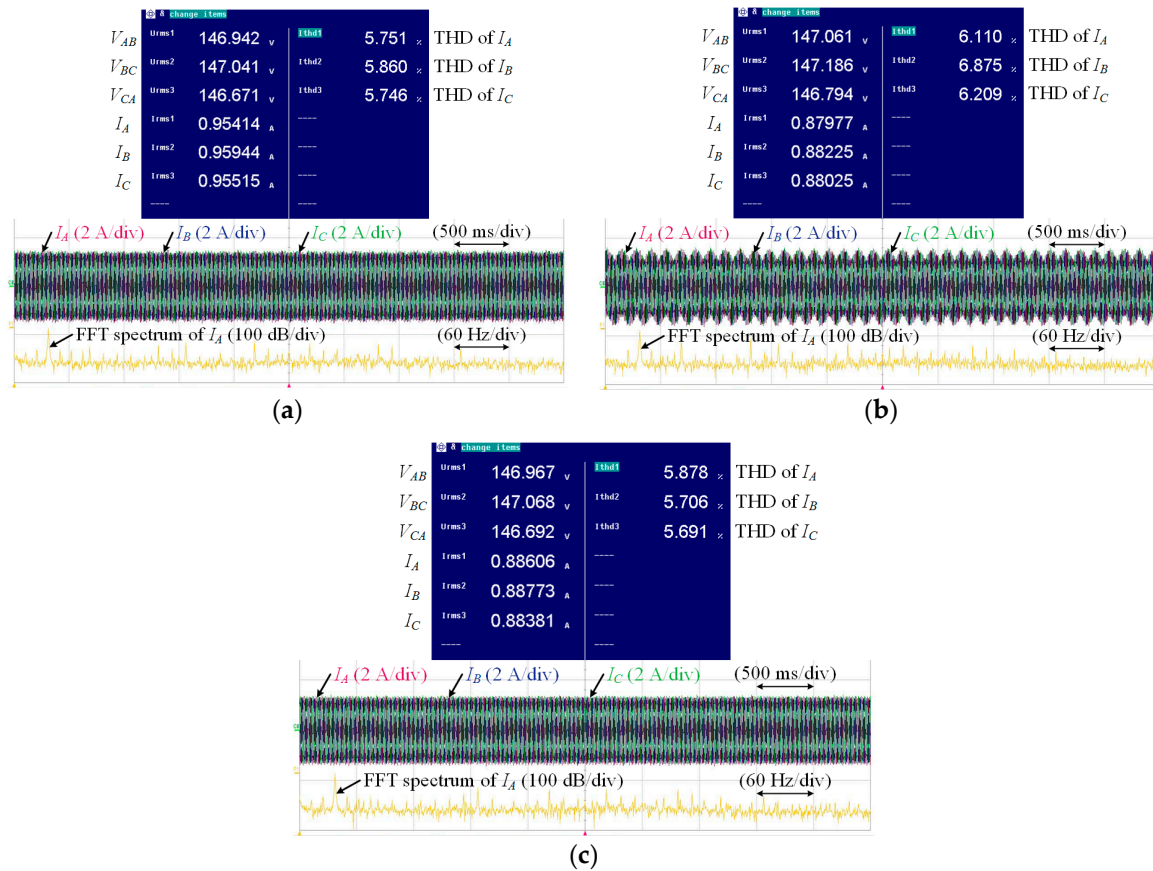

Figure 18. Experimental results of THD analysis for three-phase currents of CSR stage. (**a**) Under balanced grid voltage conditions with general control strategy; (**b**) under unbalanced grid voltage conditions with general control strategy; and (**c**) under unbalanced grid voltage conditions with proposed control strategy.

Figure 19a–c shows experimental results of THD analysis for the three-phase currents of the VSI stage such as I_R, I_S, and I_T and FFT spectrum of I_R. They have same scenario as that of Figures 11b, 14b and 15b, respectively. In Figure 19a, the three-phase grid such as V_R, V_S, and V_T has balanced voltage conditions. Therefore, I_R, I_S, and I_T are controlled to reference current using the general control strategy as balanced currents. However, in Figure 19b,c, the magnitude of V_R decreases to 70% compared with that of the normal state. Therefore, I_R, I_S, and I_T are distorted under unbalanced grid voltage conditions. Above all, I_S as S-phase current of the VSI stage is heavily distorted as shown in Figure 14b. Therefore, THD of I_S is increased as shown in Figure 19b. In Figure 19c, the three-phase currents of the VSI stage are controlled using the proposed control strategy for the balanced currents. As a result, THDs of I_R, I_S, and I_T are decreased.
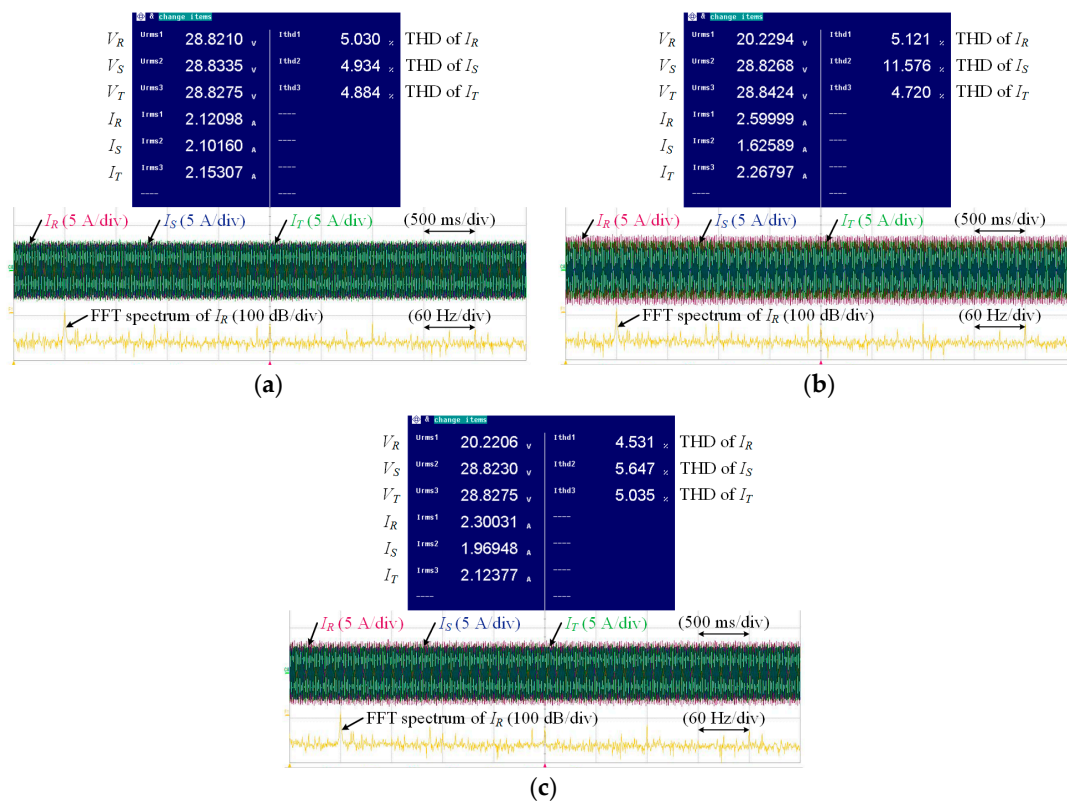
Figure 19. Experimental results of THD analysis for three-phase currents of VSI stage. (**a**) Under balanced grid voltage conditions with general control strategy; (**b**) under unbalanced grid voltage conditions with general control strategy; and (**c**) under unbalanced grid voltage conditions with proposed control strategy.

6. Conclusions

This paper proposed a control strategy for balanced currents of the CSR stage in an IMC under unbalanced grid voltage conditions. Unlike other researches, which dealt with modulation strategies under unbalanced voltage conditions of the three-phase grid connected to the CSR stage and, this paper dealt the control strategy under unbalanced voltage conditions of the three-phase grid connected to the VSI stage. The generated power from the PMSG of the GS is transmitted to a three-phase grid using an IMC as an AC-AC power conversion system. If the three-phase grid has unbalanced voltage conditions, the three-phase currents of the CSR and the VSI stages are distorted. Above all, the distorted currents of the CSR stage affect the instability of the GS. Therefore, in this paper, the positive and negative phase-sequence components of the unbalanced grid voltages and currents are used for balanced currents of the CSR stage. Using the proposed control strategy, the three-phase currents of the CSR stage are controlled to balance currents under unbalanced grid voltage conditions. Additionally, because the IMC does not have energy storage elements, the three-phase currents of the VSI stage are also controlled to balance currents. Lastly, a simulation and experimental results verify the effectiveness of the proposed control strategy.

Author Contributions: Kyo-Beum Lee provided guidance and supervision. June-Seok Lee conceived the idea of this paper and performed the simulation. Yeongsu Bak implemented the main research, performed the experiment, wrote the paper and revised the manuscript as well. All authors have equally contributed to the simulation analysis, experiment and result discussions.

Conflicts of Interest: The authors declare no conflict of interest.

References

1. Bak, Y.; Lee, E.; Lee, K.-B. Indirect matrix converter for hybrid electric vehicle application with three-phase and single-phase outputs. *Energies* **2015**, *8*, 3849–3866. [CrossRef]
2. Park, K.; Lee, K.-B.; Blaabjerg, F. Improving output performance of a Z-source sparse matrix converter under unbalanced input-voltage conditions. *IEEE Trans. Power Electron.* **2012**, *27*, 2043–2054. [CrossRef]
3. Dos Santos, E.C.; Rocha, N.; Jacobina, C.B. Suitable single-phase to three-phase AC-DC-AC power conversion system. *IEEE Trans. Power Electron.* **2015**, *30*, 860–870. [CrossRef]
4. Lee, E.; Lee, K.-B. Design and implementation of a reverse matrix converter for permanent magnet synchronous motor drives. *J. Electr. Eng. Technol.* **2015**, *10*, 2297–2306. [CrossRef]
5. Lee, E.; Lee, K.-B. Fault-tolerant strategy to control a reverse matrix converter for open-switch faults in the rectifiers stage. *J. Power Electron.* **2016**, *16*, 57–65. [CrossRef]
6. Lee, J.-S.; Lee, K.-B.; Blaabjerg, F. Open-switch fault detection method of a back-to-back converter using NPC topology for wind turbine systems. *IEEE Trans. Ind. Appl.* **2015**, *51*, 325–335. [CrossRef]
7. Heo, S.Y.; Kim, M.K.; Choi, J.W. Hybrid intelligent control method to improve the frequency support capability of wind energy conversion systems. *Energies* **2015**, *8*, 11430–11451. [CrossRef]
8. Friedli, T.; Kolar, J.W.; Rodriguez, J.; Wheeler, P.W. Comparative evaluation of three-phase AC-AC matrix converter and voltage DC-link back-to-back converter system. *IEEE Trans. Ind. Electron.* **2012**, *59*, 4487–4510. [CrossRef]
9. Jeong, H.G.; Ro, H.S.; Lee, K.-B. An improved maximum power point tracking method for wind power systems. *Energies* **2012**, *5*, 1339–1354. [CrossRef]
10. Zhang, Z.; Wang, F.; Sun, T.; Rodriguez, J.; Kennel, R. FPGA-based experimental investigation of a quasi-centralized model predictive control for back-to-back converters. *IEEE Trans. Power Electron.* **2016**, *31*, 662–674. [CrossRef]
11. Kolar, J.W.; Schafmeister, F.; Round, S.D.; Ertl, H. Novel three-phase AC-AC sparse matrix converters. *IEEE Trans. Power Electron.* **2007**, *22*, 1649–1661. [CrossRef]
12. Lee, K.-B.; Blaabjerg, F. Simple power control for sensorless induction motor drives fed by a matrix converter. *IEEE Trans. Energy Convers.* **2008**, *23*, 781–788. [CrossRef]
13. Shibata, S.; Yamada, H.; Tanaka, T.; Okamoto, M. Reduced-capacity inrush current suppressor using a matrix converter in a wind power generation system with squirrel-cage induction machines. *Energies* **2016**, *9*, 223. [CrossRef]
14. Lee, K.-B.; Blaabjerg, F. Sensorless DTC-SVM for induction motor driven by a matrix converter using a parameter estimation strategy. *IEEE Trans. Ind. Electron.* **2008**, *55*, 512–521. [CrossRef]
15. Jussila, M.; Tuusa, H. Comparison of simple control strategies of space-vector modulated indirect matrix converter under distorted supply voltage. *IEEE Trans. Power Electron.* **2007**, *22*, 139–148. [CrossRef]
16. Kwak, M.-S.; Sul, S.-K. Control of an open-winding machine in a grid-connected distributed generation system. *IEEE Trans. Ind. Appl.* **2008**, *44*, 1259–1267. [CrossRef]
17. Ko, Y.-J.; Lee, K.-B.; Lee, D.-C.; Kim, J.-M. Fault diagnosis of three-parallel voltage-source converter for a high-power wind turbine. *IET Power Electron.* **2012**, *5*, 1058–1067. [CrossRef]
18. Qiu, Y.; Zhang, W.; Cao, M.; Feng, Y.; Infield, D. An electro-thermal analysis of a variable-speed doubly-fed induction generator in a wind turbine. *Energies* **2015**, *8*, 3386–3402. [CrossRef]
19. Lee, J.-S.; Lee, K.-B. Open-circuit fault-tolerant control for outer switches of three-level rectifiers in wind turbine systems. *IEEE Trans. Power Electron.* **2016**, *31*, 3806–3815. [CrossRef]
20. Wang, L.; Lin, P.-Y. Analysis of a commercial biogas generation system using a gas engine-induction generator set. *IEEE Trans. Energy Convers.* **2009**, *24*, 230–239. [CrossRef]
21. Liu, X.; Blaabjerg, F.; Loh, P.C.; Wang, P. Carrier-Based Modulation Strategy and Its Implementation for Indirect Matrix Converter under Unbalanced Grid Voltage Conditions. In Proceedings of the International Power Electronics and Motion Control Conference and Exposition (EPE/PEMC), Novi Sad, Serbia, 4–6 September 2012; pp. LS6a.2-1–LS6a.2-7.
22. Vekhande, V.; Pimple, B.B.; Fernandes, B.G. Modulation of Indirect Matrix Converter under Unbalanced Source Voltage Condition. In Proceedings of the IEEE Energy Conversion Congress and Exposition (ECCE), Phoenix, AZ, USA, 17–22 September 2011; pp. 225–229.

23. Babaei, S.; Fardanesh, B.; Bhattacharya, S. High-power VSC-based simultaneous positive-and negative-sequence voltage regulator. *IEEE Trans. Power Deliv.* **2014**, *29*, 2124–2135. [CrossRef]
24. Nejabatkhah, F.; Li, Y.W.; Wu, B. Control strategies of three-phase distributed generation inverters for grid unbalanced voltage compensation. *IEEE Trans. Power Electron.* **2016**, *31*, 5228–5241.
25. Martinez, M.I.; Tapia, G.; Susperregui, A.; Camblong, H. DFIG power generation capability and feasibility regions under unbalanced grid voltage conditions. *IEEE Trans. Energy Convers.* **2011**, *26*, 1051–1062. [CrossRef]
26. Liu, X.; Wang, P.; Loh, P.C.; Blaabjerg, F. A compact three-phase single-input/dual-output matrix converter. *IEEE Trans. Ind. Electron.* **2012**, *59*, 6–16. [CrossRef]
27. Nguyen, T.D.; Lee, H.-H. Dual three-phase indirect matrix converter with carrier-based PWM method. *IEEE Trans. Power Electron.* **2014**, *29*, 569–581. [CrossRef]
28. Jeong, H.G.; Lee, K.-B. A control scheme to fulfill the grid-code under various fault conditions in the grid-connected wind turbines. *Electr. Eng.* **2014**, *96*, 199–210. [CrossRef]